Int. J. Electrochem. Sci., 13 **(2018)** 8817 – 8826, doi: 10.20964/2018.09.10

International Journal of
ELECTROCHEMICAL
SCIENCE
www.electrochemsci.org

Effect of Sintering time on Mn^{3+}/Mn^{4+} Ratio and Rate Capability of Spinel $Li_{1.02}Mn_2O_4$

Yang Fu[1], *Yi-Jie Gu*[1,*], *Yun-Bo Chen*[2], *Hong-Quan Liu*[1], *Zi-Zhen Xu*[1], *Wen-Li Kong*[1], *Yan-Jie Wu*[1]

[1] College of Materials Science and Engineering, Shandong University of Science and Technology, Qingdao 266510, China
[2] Advanced Manufacture Technology Center, China Academy of Machinery Science and Technology, Beijing 100044, China
[*]E-mail: 13792900643@163.com

Received: 20 March 2018 / *Accepted:* 14 June 2018 / *Published:* 5 August 2018

The spinel $Li_{1.02}Mn_2O_4$ samples were synthesized at different sintering times (5 h, 10 h, 15 h, and 20 h) via a solid-state method. The Mn^{4+} content decreases from 84.32% to 77.52% as the synthesis time increases from 5 h to 20 h, as indicated by Mn $2p_{3/2}$ X-ray photoelectron spectra. The rate capability of $Li_{1.02}Mn_2O_4$ samples increased initially and then decreased as synthesis time increased from 5 h to 20 h. Our results show that $Li_{1.02}Mn_2O_4$ sample synthesized for 10 h has the best rate capabilities of 144.1 mAh/g, 138.2 mAh/g, 126 mAh/g, and 106.2 mAh/g at 0.1, 0.2, 0.5, and 1 C, respectively. We suggest that change in rate capability of the $Li_{1.02}Mn_2O_4$ samples with increased synthesis time is related to the modification of Mn^{4+} content in $LiMn_2O_4$.

Keywords: Spinel $LiMn_2O_4$; Mn^{3+}/Mn^{4+} ratio; High-rate performance.

1. INTRODUCTION

Because $LiMn_2O_4$ cathode material has many advantages over other cathode materials, it has attracted worldwide attention [1-6]. However, spinel $LiMn_2O_4$ still has the unavoidable challenges of poor cycling retention and limited rate performance, especially the rapid capacity fade at elevated temperature, which adversely influences its potential as a cathode material for next-generation lithium-ion batteries. Capacity fading has been attributed to manganese dissolution, structural instability, and Jahn-Teller distortion [7-9], and Mn^{3+} is responsible these processes [10-12].

In addition, the change in electrochemical performance is related to the change of the second phase. The structure of the second phase has been well studied by many researchers [13-15]. In this work, we systematically studied $Li_{1.02}Mn_2O_4$ samples synthesized at different sintering times (5 h, 10

h, 15 h, and 20 h) using the same precursors prepared by the solid-state reaction method. The structure, morphology, and Mn valence state of $LiMn_2O_4$ were obtained by X-ray diffraction (XRD), scanning electron microscopy (SEM), and X-ray photoelectron spectroscopy (XPS), respectively.

2. EXPERIMENTAL

2.1. Materials synthesis

To synthesize $LiMn_2O_4$, the mixture of as-prepared Mn_3O_4 and Li_2CO_3 (molar ratio of Li:Mn = 1.02:2) was mixed with alcohol in the agate mortar, and calcined at 500 °C for 5 h and then synthesized at 750 °C for different times (5 h, 10 h, 15 h, 20 h). Finally, a black powder ($LiMn_2O_4$) was obtained. Pristine Mn_3O_4 and Li_2CO_3 were obtained from industrial manufacturers.

2.2. Characterization of materials

The structure of the $LiMn_2O_4$ was characterized by powder X-ray diffraction (XRD, D/Max2500PC, Japan) with a tube voltage of 30 kV, a tube current of 100 mA, and a 2θ scan range of 10–120° with a step size of 0.02°. The morphology and microstructure of the samples were studied using field-emission scanning electron microscopy (FESEM, Nova Nano SEM450, USA). X-ray photoelectron spectroscopy (XPS) was performed using Thermo Scientific ESCALAB 250 XI with a monochromatic Al Kα (1350.08 eV) anode (250 W, 10 kV, 30 mA).

2.3. Electrochemical measurements

The as-synthesized $LiMn_2O_4$, carbon black, and polyvinylidene fluoride were mixed at a weight ratio of 85:10:5 in N-methyl-2-pyrrolidone to form a slurry. Charge/discharge tests were performed over a voltage range of 3.0–4.3 V with a battery test system (LAND-CT2001A, China). EIS was performed using an impedance analyzer (Zahner Elektrik IM6, Germany) over a frequency range of 100 mHz to 100 kHz with amplitude of 10 mV.

3. RESULTS AND DISCUSSION

Figure 1 shows the XRD patterns of $Li_{1.02}Mn_2O_4$ samples synthesized over time periods of 5 h, 10 h, 15 h, or 20 h. The XRD patterns of the four samples are in agreement with the standard pattern of spinel $LiMn_2O_4$. The structures of all four samples are with high degrees of crystallinity. The intensity ratio of the (311) and (400) peaks (I(311)/I(400)) of the four samples are 1.007 for 5 h, 0.959 for 10 h, 0.949 for 15 h and 0.916 for 20 h, indicating that I(311)/I(400) decreased with increasing synthesis time. The intensity ratio I(311)/I(400) is related to the electrochemical performance [16]. Therefore, optimizing the synthesis time may improve the electrochemical performance of the $Li_{1.02}Mn_2O_4$ samples.

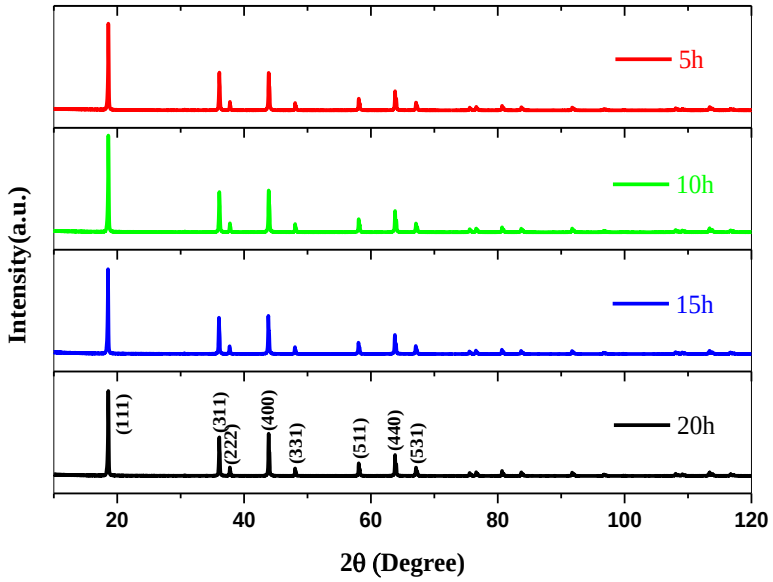

Figure 1. XRD patterns of $Li_{1.02}Mn_2O_4$ samples synthesized at different sintering times (5 h, 10 h, 15 h, and 20 h).

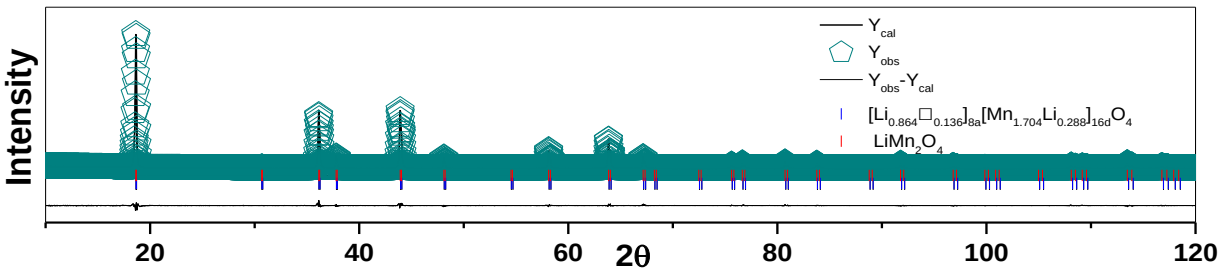

Figure 2. Rietveld refinement of XRD patterns of $Li_{1.02}Mn_2O_4$ sample synthesized for 5 h.

Table 1. The structural parameters determined for the $Li_{1.02}Mn_2O_4$ materials synthesized at different sintering times (5 h, 10 h, 15 h, and 20 h) from the refinement of the XRD data. ($Li_2Mn_3O_7$ is an abbreviated form of $[Li_{0.864}\square_{0.136}]_{8a}[Mn_{1.704}Li_{0.288}]_{16d}O_4$)(The data of 10h sample has been published in previous paper [8])

	5h		10h		15h		20h	
	$LiMn_2O_4$	$Li_2Mn_3O_7$	$LiMn_2O_4$	$Li_2Mn_3O_7$	$LiMn_2O_4$	$Li_2Mn_3O_7$	$LiMn_2O_4$	$Li_2Mn_3O_7$
Lattice constants								
a(Å)	8.23952(7)	8.2333(5)	8.24489(7)	8.2384(5)	8.23773(7)	8.2310(5)	8.23963(8)	8.2346(6)
Cell volume ($Å^3$)	559.378(0.008)	558.104(0.059)	560.472(0.008)	559.158(0.065)	559.015(0.008)	557.644(0.061)	559.401(0.009)	558.375(0.065)
Structure parameters								
R_p	7.85		7.10		8.04		8.65	
R_{wp}	11.9		10.2		12.2		12.5	
Li_{8a}								
X	0.12500(0)	0.12500(0)	0.12500(0)	0.12500(0)	0.12500(0)	0.12500(0)	0.12500(0)	0.12500(0)
Y	0.12500(0)	0.12500(0)	0.12500(0)	0.12500(0)	0.12500(0)	0.12500(0)	0.12500(0)	0.12500(0)

Z	0.12500(0)	0.12500(0)	0.12500(0)	0.12500(0)	0.12500(0)	0.12500(0)	0.12500(0)	0.12500(0)
B	0.019(204)	0.500(0)	0.361(194)	0.500(0)	0.234(223)	0.500(0)	0.198(249)	0.500(0)
SOF	1.00000(0)	0.86414(0)	1.00000(0)	0.86414(0)	1.00000(0)	0.86414(0)	1.00000(0)	0.86414(0)
Mn_{16d}								
X	0.50000(0)	0.50000(0)	0.50000(0)	0.50000(0)	0.50000(0)	0.50000(0)	0.50000(0)	0.50000(0)
Y	0.50000(0)	0.50000(0)	0.50000(0)	0.50000(0)	0.50000(0)	0.50000(0)	0.50000(0)	0.50000(0)
Z	0.50000(0)	0.50000(0)	0.50000(0)	0.50000(0)	0.50000(0)	0.50000(0)	0.50000(0)	0.50000(0)
B	0.372(17)	0.500(0)	0.387(15)	0.500(0)	0.399(18)	0.500(0)	0.388(21)	0.500(0)
SOF	1.0000(0)	0.85214(0)	1.0000(0)	0.85214(0)	1.0000(0)	0.85214(0)	1.0000(0)	0.85214(0)
Li_{16d}								
X		0.50000(0)		0.50000(0)		0.50000(0)		0.50000(0)
Y		0.50000(0)		0.50000(0)		0.50000(0)		0.50000(0)
Z		0.50000(0)		0.50000(0)		0.50000(0)		0.50000(0)
B		0.500(0)		0.500(0)		0.500(0)		0.500(0)
SOF		0.14402(0)		0.14402(0)		0.14402(0)		0.14402(0)
O_{32e}								
X	0.26155(16)	0.26672(201)	0.26159(15)	0.27836(270)	0.26174(17)	0.27685(264)	0.26158(18)	0.27072(245)
Y	0.26155(16)	0.26672(201)	0.26159(15)	0.27836(270)	0.26174(17)	0.27685(264)	0.26158(18)	0.27072(245)
Z	0.26155(16)	0.26672(201)	0.26159(15)	0.27836(270)	0.26174(17)	0.27685(264)	0.26158(18)	0.27072(245)
B	0.963(50)	0.500(0)	1.131(45)	0.500(0)	0.959(52)	0.500(0)	0.973(57)	0.500(0)
SOF	1.00000(0)	1.00000(0)	1.00000(0)	1.00000(0)	1.00000(0)	1.00000(0)	1.00000(0)	1.00000(0)

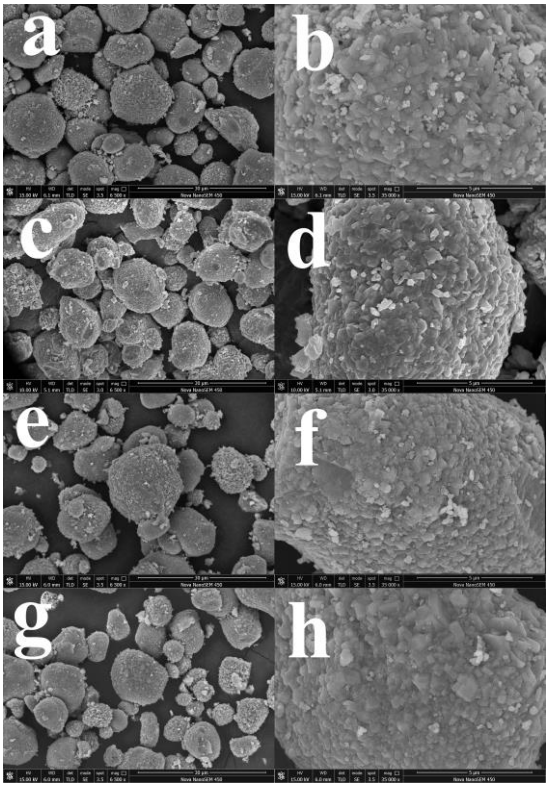

Figure 3. SEM micrographs of $Li_{1.02}Mn_2O_4$ samples synthesized at different sintering times (5 h, 10 h, 15 h, and 20 h) (a,b): 5 h; (c,d): 10 h; (e,f): 15 h; (g,h): 20 h.

The structural parameters of the $Li_{1.02}Mn_2O_4$ materials synthesized at different sintering times determined from the refinement of the XRD data are given in Table 1, which indicates that $[Li_{0.864}\square_{0.136}]_{8a}[Mn_{1.704}Li_{0.288}]_{16d}O_4$ exists in all four $Li_{1.02}Mn_2O_4$ samples. Rietveld refinement of XRD patterns of $Li_{1.02}Mn_2O_4$ sample synthesized for 5 h is given in Fig. 2, and different colors indicate the two phases in the $Li_{1.02}Mn_2O_4$ sample.

The morphologies and microstructures of the four $Li_{1.02}Mn_2O_4$ samples were investigated using SEM (Fig. 3). Under high magnification, it was observed that particles were composed of nano-polyhedrons with well-defined edges and planes, and that these polyhedrons have grown together on the plane. Similar morphologies and particle sizes were shown by SEM images for all samples, reflecting that synthesis time did not affect the morphology of $LiMn_2O_4$ materials.

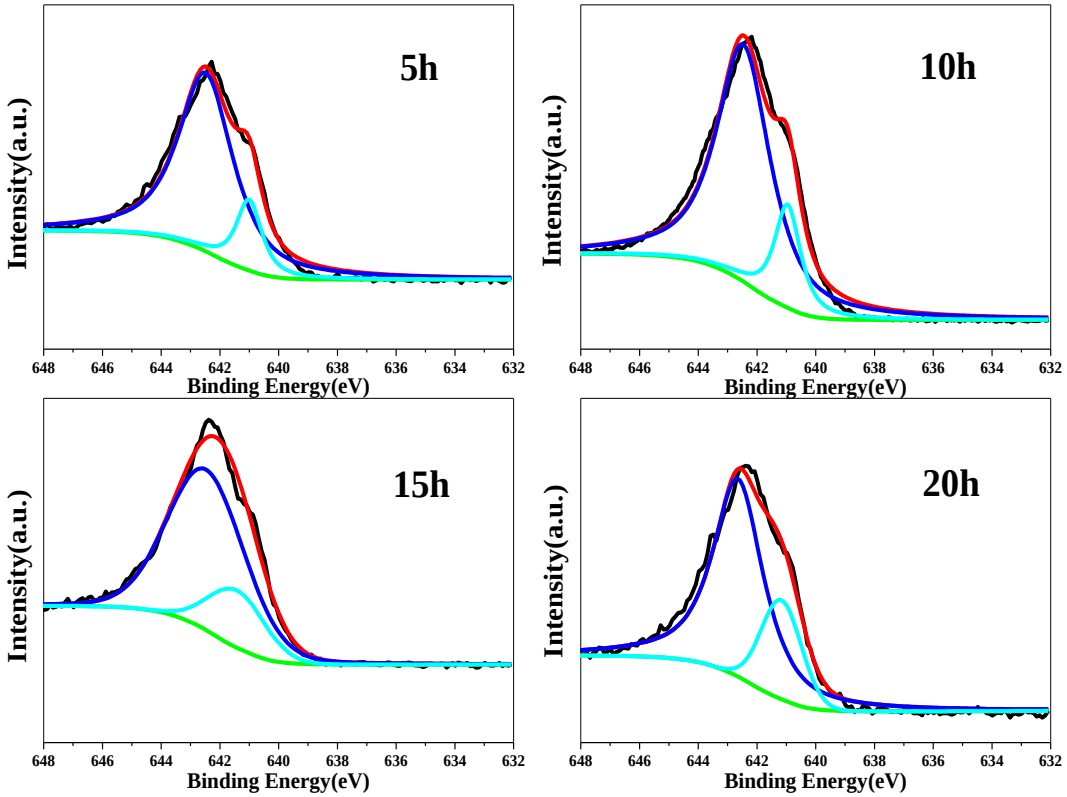

Figure 4. Deconvoluted profile of specific Mn $2p_{3/2}$ XPS spectra of $Li_{1.02}Mn_2O_4$ samples synthesized at different sintering times (5 h, 10 h, 15 h, and 20 h).

The valence states of transition metal Mn in as-synthesized $Li_{1.02}Mn_2O_4$ samples were examined by XPS measurements (Fig. 4). The Mn $2p_{3/2}$ XPS binding energies for Mn^{3+} and Mn^{4+} was 641 eV(Mn_2O_3) and 642.4 eV(MnO_2), respectively (Table 2). The Mn^{4+} content of gradually decreased from 84.32% to 77.52% as synthesis time increased from 5 h to 20 h, indicating that the content of $[Li_{0.864}\square_{0.136}]_{8a}[Mn_{1.704}Li_{0.288}]_{16d}O_4$ decreased gradually as well (Fig. 5). The results also showed that

the average valence of Mn changed from 3.8432 to 3.7752 (Table 2). $[Li_{0.864}\square_{0.136}]_{8a}[Mn_{1.704}Li_{0.288}]_{16d}O_4$ suppressed the formation of a surface passivation film between the cathode material and the electrolyte, thereby improving the electrochemical performance.

Table 2. Binding energy, cation distribution, and average valence of Mn from XPS (Mn-$2p_{3/2}$ spectra) of $Li_{1.02}Mn_2O_4$ samples.

Sample	Binding energy(eV)		Cation distribution		Average valence
	Mn^{4+}	Mn^{3+}	Mn^{4+} (%)	Mn^{3+} (%)	Mn
5h	642.482	641.002	84.32	15.68	3.8432
10h	642.460	640.956	82.42	17.58	3.8242
15h	642.462	641.425	80.23	19.77	3.8023
20h	642.640	641.170	77.52	22.48	3.7752

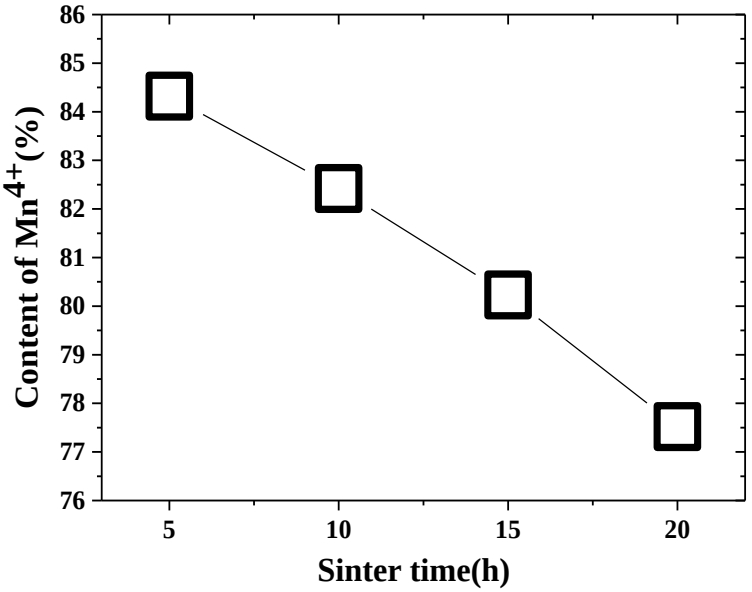

Figure 5. The Mn^{4+} content of $Li_{1.02}Mn_2O_4$ samples synthesized at different sintering times (5 h, 10 h, 15 h, and 20 h).

The first charge-discharge curves of $Li_{1.02}Mn_2O_4$ samples in the voltage range of 3.0–4.3 V at a rate of 0.1 C are given in Fig. 6. Two plateaus associated with two steps of the lithium extraction (or insertion) were observed in all samples. The $Li_{1.02}Mn_2O_4$ sample synthesized for 10 h showed the highest discharge capacity (144.1 mAh/g). For synthesis times of 5 h, 15 h, and 20 h, the discharge capacities were 140.6 mAh/g, 134.5 mAh/g, and 136 mAh/g, respectively.

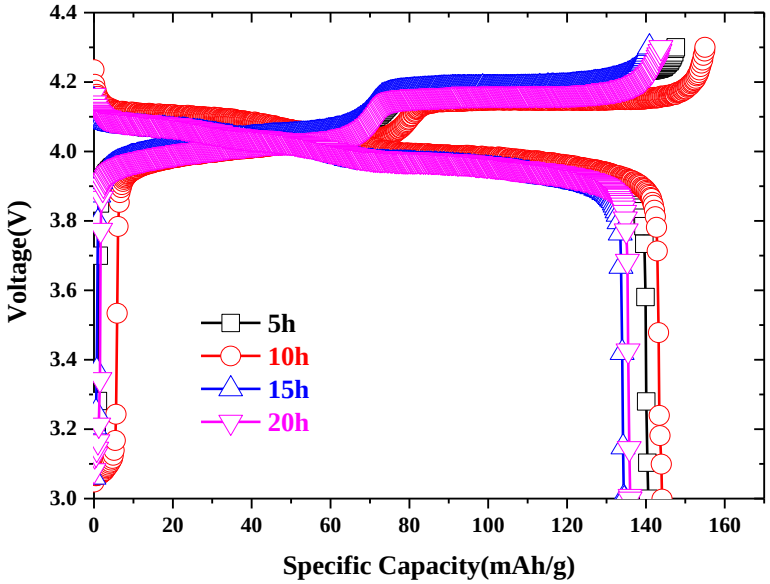

Figure 6. The charge-discharge curves of $Li_{1.02}Mn_2O_4$ samples synthesized at different sintering times (5 h, 10 h, 15 h, and 20 h) between 3.0 V to 4.3 V at a rate of 0.1 C.

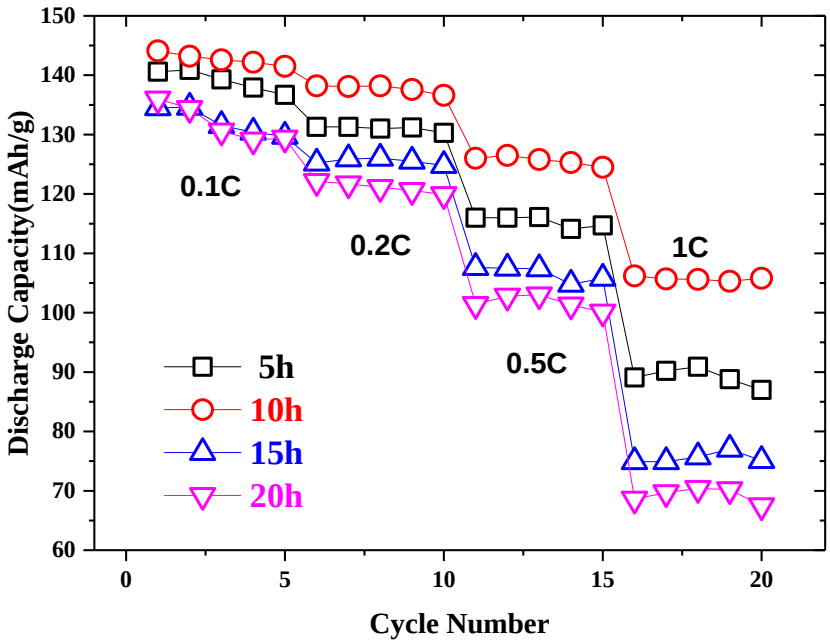

Figure 7. Rate capability of $Li_{1.02}Mn_2O_4$ samples synthesized at different sintering times (5 h, 10 h, 15 h, and 20 h) at 25 ^{o}C.

The rate capabilities of the four samples after 5 cycles at current rates ranging from 0.1 C to 1 C are presented in Fig. 7. The charge and discharge process was in the voltage range of 3.0–4.3 V at the same current rate. The specific capacity of all the samples decreased by varying degrees with the

increase in current rate due to the enhancement of cell polarization [17]. The results indicated that $Li_{1.02}Mn_2O_4$ sample synthesized for 10 hours has the best rate capability of 144.1 mAh/g, 138.2 mAh/g, 126 mAh/g, and 106.2 mAh/g at rates of 0.1, 0.2, 0.5 and 1 C, respectively. The results indicated that the discharge capacity of $Li_{1.02}Mn_2O_4$ samples increased from 89.1 mAh/g to 106.2 mAh/g and then decreased from 106.2 mAh/g to 68.6 mAh/g at a rate of 1 C as the synthesis time increased from 5 h to 20 h. The results show that the rate capability of the $LiMn_2O_4$ samples decreases as the synthesis time increases from 5 h to 20 h (Fig. 7) due to the decrease in $[Li_{0.864}\square_{0.136}]_{8a}[Mn_{1.704}Li_{0.288}]_{16d}O_4$ content. The Mn^{4+} content is the highest when the synthesis time is 5 h, which indicates that the $[Li_{0.864}\square_{0.136}]_{8a}[Mn_{1.704}Li_{0.288}]_{16d}O_4$ content in the 5 h sample is the highest, but the rate capability of 5 h sample is poor. Because the $[Li_{0.864}\square_{0.136}]_{8a}[Mn_{1.704}Li_{0.288}]_{16d}O_4$ has a high lithium content, the main phase is lithium deficient, and this results in poor rate performance.

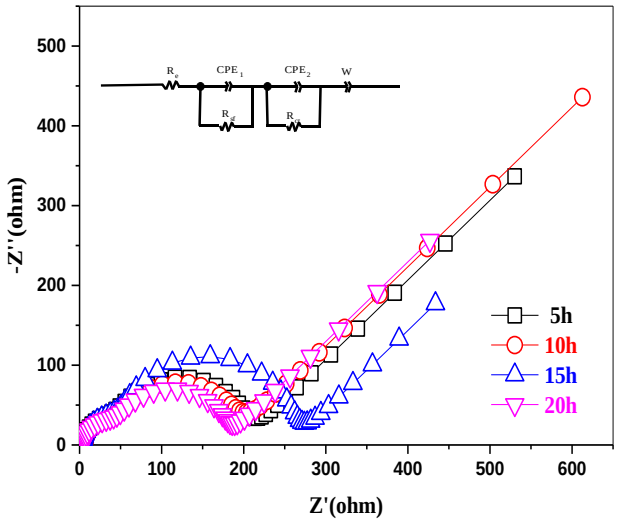

Figure 8. Electrochemical impedance spectroscopy of $Li_{1.02}Mn_2O_4$ samples synthesized at different sintering times (5 h, 10 h, 15 h, and 20 h) with an amplitude of 10 mV.

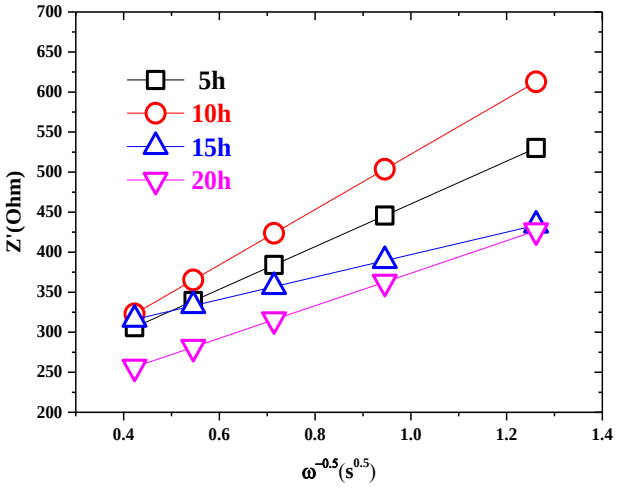

Figure 9. Z' vs. $\omega^{-0.5}$ plots at the low frequency region for $Li_{1.02}Mn_2O_4$ samples synthesized at different sintering times (5 h, 10 h, 15 h, and 20 h).

Table 3. R_e, R_{sf}, R_{ct}, and D_{Li}^+ for $Li_{1.02}Mn_2O_4$ samples synthesized at different sintering times (5 h, 10 h, 15 h, and 20 h).

Time/h	$R_e(\Omega)$	$R_{sf}(\Omega)$	$R_{ct}(\Omega)$	$D_{Li}^+(cm^2s^{-1})$
5h	3.318	150.5	39.53	9.34×10^{-16}
10h	5.912	37.84	133.1	5.57×10^{-16}
15h	3.467	209.3	43.84	3.38×10^{-15}
20h	4.707	39.97	125.9	1.61×10^{-15}

Figure 8 displays the Nyquist plots of $Li_{1.02}Mn_2O_4$ samples synthesized at different sintering times after 5 cycles at a rate of 0.1 C in a fully discharged state. The equivalent circuit is also shown in the inset of Fig. 8. The diffusion coefficient D_{Li}^+ is calculated according to the following equation [18-20]:

$$D_{Li}^+ = \frac{R^2T^2}{2A^2n^4F^4c^2\sigma^2}$$

where R is the gas constant (8.314 J $mol^{-1}K^{-1}$), T is the temperature (298.15 K), A is the surface area of the electrode, n is the number of shifted electrons, F is the Faraday constant (96,500 C mol^{-1}), c is the molar concentration of lithium ions, and the plot slope of Z' vs. $\omega^{-0.5}$ gives **σ**, the Warburg coefficient [21-23]. The plot of the real part of the impedance Z' vs. $\omega^{-0.5}$ in the low-frequency region for the $Li_{1.02}Mn_2O_4$ samples synthesized for different time periods is displayed in Fig. 9. The R_e, R_{sf}, and R_{ct} values simulated by Zsimpwin software for $LiMn_2O_4$ samples are listed in Table 3. The results showed that the sample synthesized for 15 h had the largest R_{sf} value of 209.3 Ω, while the sample synthesized over 10 h had the largest R_{ct} value of 133.1 Ω. In addition, the sample synthesized over 15 h had the largest D_{Li}^+ value of 3.38×10^{-15}.

4. CONCLUSIONS

As the synthesis time increases from 5 h to 20 h, the Mn^{4+} content decreases from 84.32% to 77.52%. The rate capability of the $Li_{1.02}Mn_2O_4$ samples increase initially and then decrease as the synthesis time increases from 5 h to 20 h. The refinement result shows that there is the $[Li_{0.864}\square_{0.136}]_{8a}[Mn_{1.704}Li_{0.288}]_{16d}O_4$ in the $Li_{1.02}Mn_2O_4$ samples synthesized at different sintering times (5 h, 10 h, 15 h, and 20 h). Our results demonstrate the relationship between Mn^{4+} content and the rate capability of the $Li_{1.02}Mn_2O_4$ cathode materials.

ACKNOWLEDGEMENTS

This work was financially supported by National Natural Science Foundation of China (No. 51641206), Postdoctoral Science Foundation of China (2013M541907) and special funds for independent innovation and transformation of achievements in Shandong Province (Grant No. 2014CGZH0911).

References

1. L. He, S.C. Zhang, X. Wei, Z.J. Du, G.R. Liu and Y.L. Xing, *J. Power Sources*, 220 (2012) 228.
2. D. Zhan, F. Yang, Q.G. Zhang, X.H. Hua and T.Y. Peng, *Electrochim. Acta*, 129 (2014) 364.
3. O.K. Park, Y. Cho, S. Lee, H.C. Yoo, H.K. Song and J. Cho, *Energ. Environ. Sci*, 4 (2011) 1621.
4. X.Y. Qiu, Q.C. Zhuang, Q.Q. Zhang, R. Cao, P.Z. Ying, Y.H. Qiang and S.G. Sun, *Phys. Chem. Chem. Phys.*, 14 (2012) 2617.
5. H.J. Noh, S. Youn, C.S. Yoon and Y.K. Sun, *J. Power Sources*, 233 (2013) 121.
6. H.B. Liu, C. Miao, Y. Meng, Q. Xu, X.H. Zhang and Z.Y. Tang, *Electrochim. Acta*, 135 (2014) 311.
7. G.G. Amatucci, C.N. Schmutz, A. Blyr, C. Sigala, A.S. Gozdz, D. Larcher and J.M. Tarascon, *J. Power Sources*, 69 (1997) 11.
8. Y. Fu, Y.J. Gu, Y.B. Chen, H.Q. Liu and H.H. Zhou, *Solid State Ionics*, 320 (2018) 16.
9. T. Ohzuku, J. Kato, K. Sawai and T. Hirai, *J. Electrochem. Soc*., 138 (1991) 2556.
10. D.H. Jang, Y.J. Shin and S.M. Oh, *J. Electrochem. Soc*., 143 (1996) 2204.
11. A.D. Kock, E. Ferg and R.J. Gummow, *J. Power Sources*, 70 (1998) 247.
12. J. Morales, L. Sanchez and J.L. Tirado, *J. Solid State Electrochem*., 2 (1998) 420.
13. Z.L. Xu, J.B. Wang, X.J. Quan, S.J. Hu and Q.G. Wu, *J. Power Sources*, 248 (2014) 1201.
14. K. Oikawa, T. Kamiyama, F. Izumi, B.C. Chakoumakos and H. Ikuta, *Solid State Ionics*, 109 (1998) 35.
15. M.M. Thackeray, A.D. Kock and W. David, *J. Materials Research Bulletin*, 28 (1993) 1041.
16. H.Y. Zhao, F. Li, X.Q. Liu, C. Cheng and Z. Zhang, *Electrochim. Acta*, 151 (2015) 263.
17. C.H. Zheng, X. Liu, Z.F. Wu, Z.D. Chen and D.L. Fang, *Electrochim. Acta*, 111 (2013) 192.
18. J.S. Gnanaraj, V.G. Pol, A. Gedanken and D. Aurbach, *J. Electrochem. Commun*., 5 (2003) 940.
19. J. Fan and P.S. Fedkiw, *J. Power Sources*, 72 (1998) 165.
20. Y.L. Ma, Y.Z. Gao, P. J. Zuo, X.Q. Cheng and G.P. Yin, *Int. J. Electrochem. Sci*., 7 (2012) 11001.
21. Y. Huang, F.M. Jin, F.J. Chen and L. Chen, *J. Power Sources*, 256 (2014) 1.
22. Z.Q. Huo, Y.T. Cui, D. Wang, Y. Dong and L. Chen, *J. Power Sources*, 245 (2014) 331.
23. Y. Cui, X.L. Zhao and R.S. Guo, *Electrochim. Acta*, 55 (2010) 922.